Journal of Materials Chemistry A

PAPER

View Article Online
View Journal | View Issue

Cite this: J. Mater. Chem. A, 2015, 3, 22695

Integrated molecular, morphological and interfacial engineering towards highly efficient and stable solution-processed small molecule solar cells†

Jie Min,‡*[a] Yuriy N. Luponosov,‡*[b] Nicola Gasparini,[a] Lingwei Xue,[c] Fedor V. Drozdov,[b] Svetlana M. Peregudova,[d] Petr V. Dmitryakov,[e] Kirill L. Gerasimov,[f] Denis V. Anokhin,[fg] Zhi-Guo Zhang,[c] Tayebeh Ameri,[a] Sergei N. Chvalun,[be] Dimitri A. Ivanov,[fh] Yongfang Li,[c] Sergei A. Ponomarenko[bi] and Christoph J. Brabec[aj]

The synthesis of a series of A–π–D–π–A oligomers bearing coplanar electron-donating dithieno[3,2-*b*:2′,3′-*d*]silole (DTS) unit linked through bithiophene π-bridges with the electron-withdrawing alkyldicyanovinyl (alkyl-DCV) groups is described. This study demonstrates a systematic investigation of structure–property relationships in this type of oligomer and shows obvious benefits of alkyl-DCV groups as compared to the commonly used DCV ones, in terms of elaboration of high performance organic solar cells (OSCs). Considerable efforts have been made to improve the power conversion efficiency (PCE) of oligomer-based OSCs by diverse strategies including fine-tuning of the oligomer properties *via* variation of their terminal and central alkyl chains, blend morphology control *via* solvent vapor annealing (SVA) treatment, and surface modification *via* interfacial engineering. These efforts allowed achieving PCEs of up to 6.4% for DTS(Oct)$_2$-(2T-DCV-Me)$_2$ blended with PC$_{70}$BM. Further morphological investigations demonstrated that the usage of SVA treatment indeed effectively results in increased absorption and ordering of the BHJ composite, with the only exception for the most soluble oligomer DTS(Oct)$_2$-(2T-DCV-Hex)$_2$. Besides, a detailed study analyzed the charge transport properties and recombination loss mechanisms for these oligomers. This study not only revealed the importance of integrated alkyl chain engineering on gaining morphological control for high performance OSCs, but also exhibited a clear correlation between molecular ordering and charge carrier mobility respective to carrier dynamics. These results outline a detailed strategy towards a rather complete characterization and optimization methodology for organic photovoltaic devices, thereby paving the way for researchers to easily find the performance parameters adapted for widespread applications.

Received 25th August 2015
Accepted 22nd September 2015

DOI: 10.1039/c5ta06706e

www.rsc.org/MaterialsA

1. Introduction

Organic photovoltaic (OPV) devices utilizing small molecules attract the attention of researchers due to their well-defined molecular structures and high reproducibility in combination with their potential to obtain high power conversion efficiencies (PCEs) as well as low fabrication costs achievable *via* solution-processing methods.[1] The dynamic development in small molecule organic solar cells (SMOSCs) has recently led to PCEs

[a]*Institute of Materials for Electronics and Energy Technology (I-MEET), Friedrich-Alexander-University Erlangen-Nuremberg, Martensstraße 7, 91058 Erlangen, Germany. E-mail: Min.Jie@ww.uni-erlangen.de*

[b]*Enikolopov Institute of Synthetic Polymeric Materials of the Russian Academy of Sciences, Profsoyuznaya St. 70, Moscow 117393, Russia. E-mail: luponosov@ispm.ru*

[c]*CAS Key Laboratory of Organic Solids, Institute of Chemistry, Chinese Academy of Sciences, Beijing 100190, China*

[d]*Nesmeyanov Institute of Organoelement Compounds, Russian Academy of Sciences, Vavilova St. 28, Moscow, 119991, Russia*

[e]*National Research Centre "Kurchatov Institute", 1, Akademika Kurchatova pl., Moscow, 123182, Russia*

[f]*Moscow State University, Faculty of Fundamental Physical and Chemical Engineering, GSP-1, 1-51 Leninskie Gory, Moscow, 119991, Russia*

[g]*Institute for Problems of Chemical Physics, Russian Academy of Sciences, Semenov Prospect 1, Chernogolovka, Moscow Region, 142432, Russia*

[h]*Institut de Sciences des Matériaux de Mulhouse (CNRS UMR7361), 15 rue Jean Starcky, B.P 2488, Mulhouse, 68057, France*

[i]*Chemistry Department, Moscow State University, Leninskie Gory 1-3, Moscow 119991, Russia*

[j]*Bavarian Center for Applied Energy Research (ZAE Bayern), Haberstraße 2a, 91058 Erlangen, Germany*

† Electronic supplementary information (ESI) available. See DOI: 10.1039/c5ta06706e

‡ These two first authors contributed equally.

over 9%, *i.e.* comparable to those of polymer-based devices in the most promising bulk heterojunction (BHJ) configuration.[2,3]

A highly functional molecular design of D–A small molecules requires the parallel optimization of multiple properties, like engineering of the suitable band gap and suitable molecular energy levels, enhancing charge transport, achieving sufficient solubility in non-halogenated solvents, guaranteeing high absorptivity in thin films as well as excellent photochemical stability, *etc.* Thus, in order to meet simultaneously all these specific requirements, the structural components in small molecule donor materials, including donor units, acceptor units, conjugated π-bridges, heteroatom substitutions, alkyl side chains and/or pendant chains, should be designed and modified very carefully.[4–6] The creative design and choice of suitable components have successfully driven the relative efficiency to record highs.[1–3,7] Grafting of alkyl side chains with various lengths onto the small molecule backbone can dramatically influence intermolecular packing and the blend morphology and has already been shown to be an essential design criterion for the device performance.[8–10] However, the correlation between the microstructure on the one hand and the physical and photovoltaic performance on the other hand, as a function of either side or terminal alkyl chain length, is still a major puzzle, which requires more detailed studies.

Apart from a smart molecular design, microstructure engineering is one of the key strategies to achieve well-ordered and crystalline domains, allowing further reduction of bimolecular recombination losses. It is well known that an excessive dispersion of donor (D) or acceptor (A) phases can result in enhanced bimolecular recombination as well as in the formation of unbalanced charge carrier mobilities. Recently, various parameters and methods were used to control the morphology of D:A BHJ systems such as thermal annealing,[9,11] solvent vapor annealing (SVA),[3,12a] solvent additives,[11,13] mixed solvents,[14] post-additive soaking,[15] *etc.* The main goal of these procedures is to obtain a favorable photoactive layer morphology achieving large interfacial areas for efficient exciton splitting and charge separation while still guaranteeing sufficient charge transport pathways to the electrodes.[16] Among these techniques, the SVA treatment was frequently reported as the most effective processing technique to optimize the efficiency of SMOSCs.[3,12a,16] However, despite the recent positive gains in efficiency for some of the most efficient SMOSCs using SVA treatments, there is still no evidence that it can be universally applied to all kinds of small molecule systems. In fact, we will show that SVA strategies are failing in the situation of similar solubility for the D and A components.

It is well known that the non-ideal molecular structure of small molecules and their poor BHJ morphology normally showed significant charge carrier recombination losses and consequently resulted in low photovoltaic performance. Besides bulk recombination,[1,4,17,18] surface recombination is a further limiting loss mechanism for high performance OPV devices and was recently proven to be much more relevant than originally suggested.[19] Suitable interface layers are necessary to enable the loss-free extraction of the respective carriers at a rate higher than the bimolecular recombination rate.[20,21] Recently, zinc oxide (ZnO) and poly[(9,9-bis(3′-(*N*,*N*-dimethylamino)propyl)-2,7-fluorene)-*alt*-2,7-(9,9-dioctylfluorene)] (PFN) as electron transporting layers (ETLs) have been successfully applied in

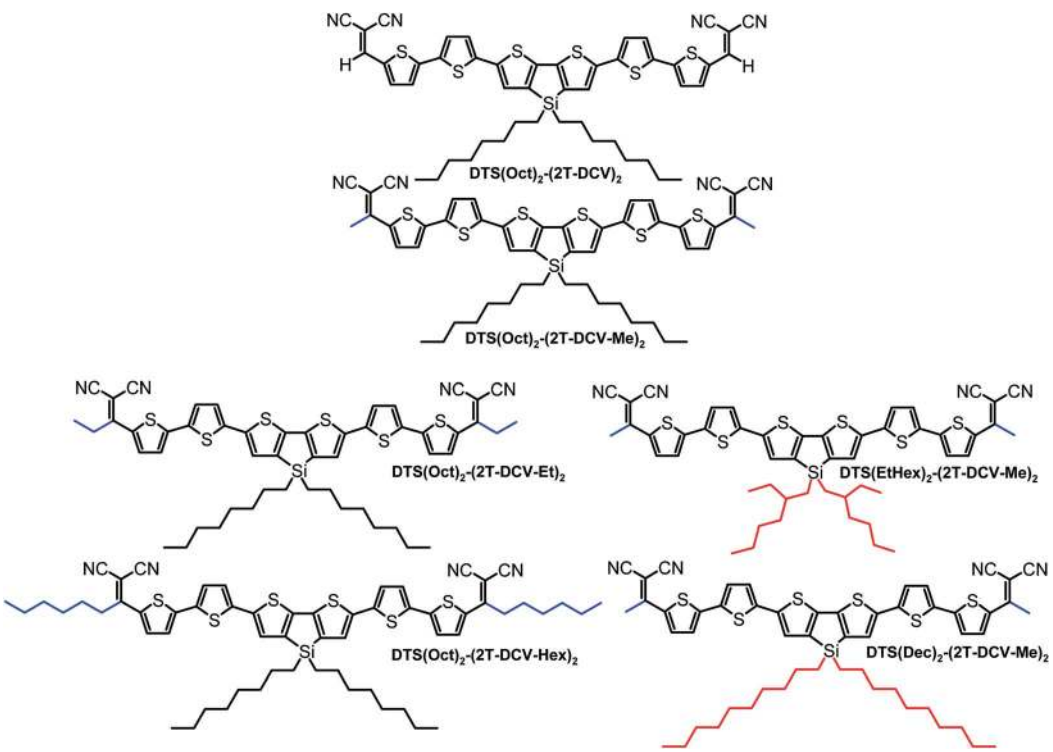

Scheme 1 Chemical structures of the DTS-based linear oligomers synthesized and investigated.

small molecule conventional solar cells with Al as a cathode.[2,22] Moreover, in our previous work, a more stable conventional architecture with the Ag cathode was presented by using an amine group functionalized fullerene complex (DMAPA-C60) as an ETL.[23] However, as compared to its polymeric counterparts, the development of interface layers applied in small molecule systems has largely been overlooked until recently. Therefore, the development of stable and effective device architectures based on interfacial engineering should be also highlighted in the photovoltaic optimization of SMOSCs.

In this work, we first report on synthesis and systematic investigation of a series of novel A–π–D–π–A oligomers based on dithieno(3,2-*b*;2′,3′-*d*)silole (DTS) as the donor unit linked through bithiophene π-bridges with alkyldicyanovinyl (alkyl-DCV) acceptor groups (Scheme 1). The oligomers differ by their alkyl groups at the central DTS and terminal DCV units. The oligomer without an alkyl group at the DCV unit ($DTS(Oct)_2$-$(2T\text{-}DCV)_2$) was synthesized as well in order to evaluate the benefits of alkyl-DCV electron-withdrawing groups as compared to common DCV ones. Secondly, the effect of SVA treatment on the BHJ morphology and device performance was systematically examined within this series of DTS-based oligomers having various solubility values. Finally, a new stable conventional architecture of OSC devices is introduced by using a solution-processed perylene diimide (PDINO) as a cathode interface layer. Emphasis will be placed on discussing the morphology–property relationships in this series of DTS-based oligomers, by means of the microstructure investigations and the charge transport properties as well as the non-geminate recombination losses with and without SVA treatments.

2. Results and discussion

2.1 Design, synthesis and characterization

The donor–acceptor (D–A) strategy was used to design DTS-based oligomers as shown in Scheme 1. This approach results in a lower bandgap due to the orbital mixing of the donor and the acceptor units and shifts absorption strength into the long-wave region because of intramolecular charge transfer (ICT) effects.[12,24] The DTS unit was chosen as a central electron donor fragment, due to its excellent stability under ambient conditions as compared to the carbon or nitrogen-containing analogs.[25,26] Further, the highly planar structure of DTS is expected to lead to a high charge-carrier mobility. The DCV groups are among the most frequently used acceptor units to design D–A oligomers due to their cheapness, well established chemistry and strong electron-withdrawing character.[7,12] A drawback of these groups is active hydrogen at the DCV group decreasing the stability and leading to the necessity to use additional side alkyls at the oligoaryl fragment to control the solubility of materials, which in turn complicates synthesis of target molecules. Therefore, in this work, the alkyl-DCV groups were chosen as acceptor units of the oligomers since they have demonstrated increased electrochemical stability as compared to DCV ones and allow the control of thermodynamic (solubility), photophysical and electronic properties by simply adjusting the length of the alkyls.[4,13,27] In order to increase the electron donating ability and charge-carrier mobility of the oligomers under discussion, bithiophene (2T) units were used as π-bridges between DTS and alkyl-DCV units. Our recent investigations revealed that the 2T length is a good compromise between shorter (1T)[28] and longer (3T)[28,29] units in terms of sufficient solubility and absorption in the long-wave region, and simplicity of preparation. Thus, the general novelty in the design of these oligomers is the utilization of various alkyl-DCV groups instead of commonly used DCV ones, which requires a different synthetic route for their preparation. In our recent work, we have reported on the synthesis of $DTS(Oct)_2$-$(2T\text{-}DCV\text{-}Me)_2$, being the first example from this series of oligomers.[30] While the preparation and initial investigation of $DTS(Oct)_2$-$(2T\text{-}DCV\text{-}Hex)_2$ were described very recently in our studies devoted to studying the influence of the bridging heteroatom and the π-bridge length as well as the terminal alkyl-chain length on the photovoltaic properties for this type of oligomer.[18,29] Here, we report on the systematic extension of these studies consisting of five oligomers with alkyl-DCV groups, namely $DTS(Oct)_2$-$(2T\text{-}DCV\text{-}Me)_2$, $DTS(Oct)_2$-$(2T\text{-}DCV\text{-}Et)_2$, $DTS(Oct)_2$-$(2T\text{-}DCV\text{-}Hex)_2$, $DTS(EtHex)_2$-$(2T\text{-}DCV\text{-}Me)_2$ and $DTS(Dec)_2$-$(2T\text{-}DCV\text{-}Me)_2$ (Scheme 1). The oligomer with the common DCV group, $DTS(Oct)_2$-$(2T\text{-}DCV)_2$, was included for reference purposes.

The general synthetic strategy developed recently for linear molecules was extended in this work successfully for this series of oligomers (Scheme 1).[30,31] It includes several consecutive reaction stages as outlined in Scheme 2. Suzuki cross-coupling between compounds **1a–d** having both the organoboron and protected carbonyl groups and the bromine-containing derivatives of DTS (**2e–g**) gave a series of oligomers (**3**), having various alkyl chains at both DCV and DTS units in isolated yields of 82–87%. Removing the protective groups was successfully achieved by treatment of the acetal and ketals with 1 M HCl to give a poorly soluble aldehyde (**4ae**) and batch of ketones (**4**) in isolated yields of 95–99%. Finally, Knövenagel condensation between malononitrile and the oligomers with carbonyl

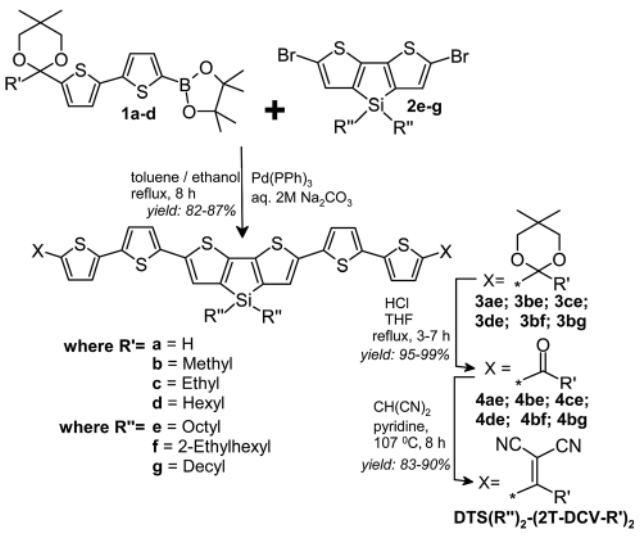

Scheme 2 Synthesis of DTS-based A–π–D–π–A oligomers.

functions in pyridine and under microwave heating gave target compounds in isolated yields of 83–90%.

^{1}H and ^{13}C-NMR spectroscopy, elemental analysis and mass-spectroscopy were used to characterize the chemical structure and purity of these molecules (see ESI, Fig. S1–S19†). The solubility of the DTS-based oligomers was measured in chloroform ($CHCl_3$) at room temperature (see Table 1). The solubility gradually increases with elongation of the alkyl chain lengths of the oligomers. Comparison of the solubility values for DTS(Oct)$_2$-(2T-DCV-Me)$_2$ and DTS(EtHex)$_2$-(2T-DCV-Me)$_2$ showed that the usage of more branched alkyl groups at the DTS unit indeed leads to increased solubility. These observations can be easily explained by a decrease of intermolecular interactions for the oligomers having longer and more branched alkyl chains, being in agreement with the their phase behavior (see below). In addition, it should be noted that DTS(Oct)$_2$-(2T-DCV)$_2$ was found to be significantly less soluble as compared to the nearest analog with the methyl-DCV groups, DTS(Oct)$_2$-(2T-DCV-Me)$_2$.

2.2 Thermal properties of the oligomers

Thermal properties of the DTS-based oligomers were investigated by thermogravimetric analysis (TGA) and differential scanning calorimetry (DSC). The results are summarized in Table 1. Thermal decomposition of the oligomers under an inert atmosphere and in air is presented in Fig. 1a and S20,† respectively. One can see that the oligomers possess very high thermal as well as thermooxidative stability. The decomposition temperature (T_d), corresponding to 5% weight losses, was found to be above 360 °C in air and above 390 °C under an inert atmosphere, as exhibited in Table 1. Residual weights vary between 40 and 65% when heating to 700 °C under nitrogen (Fig. 1a). Comparison of the weight losses at very high temperatures indicates that decomposition of the aliphatic groups is dominantly responsible for the degradation. The influence of the terminal hydrogen at the DCV unit on the thermal stability of the oligomers cannot be evaluated by this technique, since the weight loss in the case of hydrogen elimination is only around 0.2%, which is close to the experimental error.

DSC traces of the first heating are presented in Fig. 1b, while the full heating–cooling cycles are shown in Fig. S21.† All oligomers at the first heating exhibit single, sharp and strong endothermic peaks, as well as relatively high values of melting temperature (T_m) and melting enthalpy (ΔH_m), which indicates their crystalline nature.[32] The oligomer without alkyls at the DCV unit, DTS(Oct)$_2$-(2T-DCV)$_2$, has the highest T_m in this series of molecules (Table 1). However, its ΔH_m was found to be 69 J g^{-1}, which is significantly less as compared to the nearest analog with methyl-DCV terminal groups having a ΔH_m of 90 J g^{-1}. The increase of the alkyl length at the DCV unit leads to the pronounced decrease of the melting temperatures and enthalpies from 248 °C and 90 J g^{-1}, for DTS(Oct)$_2$-(2T-DCV-Me)$_2$ having the shortest alkyl chains, to 151 °C and 47 J g^{-1}, for DTS(Oct)$_2$-(2T-DCV-Hex)$_2$ having the longest terminal alkyl

Table 1 Thermal properties and solubility of the DTS-based oligomers

Compounds	Solubility[a], mg mL^{-1}	Total number of C atoms in aliphatic groups	T_m[b], °C	ΔH_m, J g^{-1}	T_d[c] (air), °C	T_d[c] (N_2), °C
DTS(Oct)$_2$-(2T-DCV)$_2$	2.5	16	259	69	378	390
DTS(Oct)$_2$-(2T-DCV-Me)$_2$	5	18	248	90	390	399
DTS(Oct)$_2$-(2T-DCV-Et)$_2$	14	20	203	58	409	410
DTS(Oct)$_2$-(2T-DCV-Hex)$_2$	24	28	152	47	360	395
DTS(EtHex)$_2$-(2T-DCV-Me)$_2$	8	18	230	76	374	390
DTS(Dec)$_2$-(2T-DCV-Me)$_2$	10	22	205	73	401	402

[a] In $CHCl_3$ at room temperature, determined by the method described in ref. 30. [b] T_m – melting temperature measured by the DSC method, ΔH – melting enthalpy. [c] T_d – decomposition temperature (at 5% weight-loss).

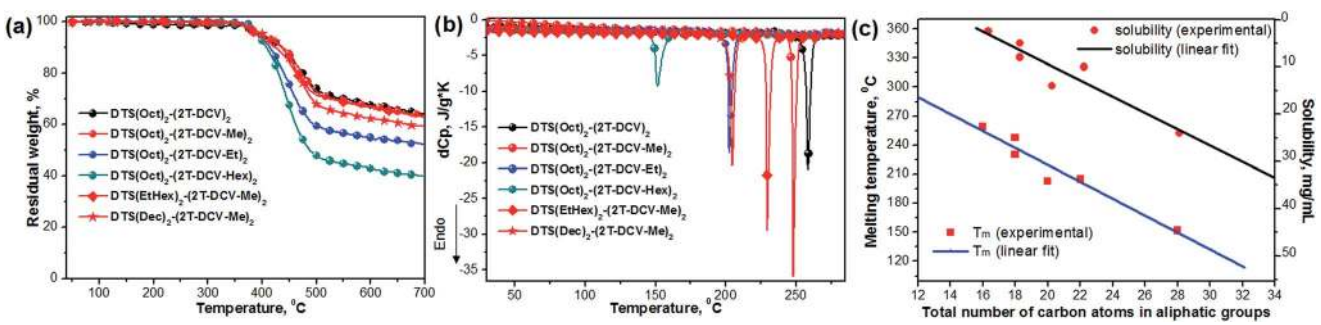

Fig. 1 (a) TGA curves under the nitrogen flow, (b) DSC first heating scans and (c) experimental and linear fitting curves of melting temperature and solubility in $CHCl_3$ *versus* the total number of carbon atoms in aliphatic groups of the molecules for the series of DTS-based oligomers investigated.

chains. Similar tendency of T_m and ΔH_m decrease can be observed also when linear octyls in DTS(Oct)$_2$-(2T-DCV-Me)$_2$ are replaced by branched 2-ethylhexyls DTS(EtHex)$_2$-(2T-DCV-Me)$_2$, while the terminal alkyls remain unchanged.

It is important to underline that melting temperature depends almost linearly on the total number of carbons atoms in aliphatic groups of the molecules regardless of their positions (Fig. 1c). Moreover, absolutely the same tendency of solubility dependence on the number of carbon atoms in aliphatic groups was observed (see Table 1 and Fig. 1c). The slight deviation from the linearity can be detected for DTS(EtHex)$_2$-(2T-DCV-Me)$_2$ having branched 2-ethylhexyls, whereas for other oligomers with straight alkyls it depends more linearly. It means that the solubility and phase behavior of these oligomers can be more or less precisely predicted and fine-tuned by simple alkyl chain engineering.

2.3 Optical and electrochemical properties

Absorption spectra in the 350–1000 nm region of the DTS-based oligomer thin films are shown in Fig. 2, and the relative optical data are summarized in Table 2. In chloroform solutions (see Fig. S22†), apart from DTS(Oct)$_2$-(2T-DCV)$_2$, the absorption spectra of these oligomers are similar and exhibit a weak peak around 387 nm corresponding to the π–π transition of the conjugated backbone, whereas the lower energy absorption band peaking at *ca.* 542 nm is ascribed to the ICT transition. Note that DTS(Oct)$_2$-(2T-DCV)$_2$ has a somewhat broader absorption spectrum with a peak maximum (λ_{max}) of 560 nm, which can be attributed to a stronger electron-withdrawing character of the DCV group as compared to the alkyl-DCV one. From solution to the film, all of the DTS-oligomers show significant red-shifts in optical absorption profiles, which indicates that there are strong intermolecular interactions leading to an aggregation in the solid-state (Fig. 2). In the series of the DTS-oligomers differing by the alkyl terminal length only, the absorption spectrum of the molecule with the longest alkyl chain, DTS(Oct)$_2$-(2T-DCV-Hex)$_2$, has the lowest red shift due to weaker intermolecular interactions of the molecules in the solid state, which is also consistent with our previous results.[4] Note that all analogs with shorter terminal alkyls possess a shoulder peak in the long wavelength region, indicating the presence of an additional ordering in films.[33,34] The strongest intensity of the shoulder peak was found for the DTS(Oct)$_2$-(2T-DCV-Me)$_2$, having the shortest terminal methyl groups and linear octyl groups at the DTS unit. Changing the octyl unit at the DTS core into either more branched 2-ethylhexyl or longer decyl groups further decreases intermolecular interactions in the solid state. Therefore, the pronounced near-IR shoulder observed for DTS(Oct)$_2$-(2T-DCV-Me)$_2$ is significantly decreased for DTS(EtHex)$_2$-(2T-DCV-Me)$_2$ and DTS(Dec)$_2$-(2T-DCV-Me)$_2$ (Fig. 2b).

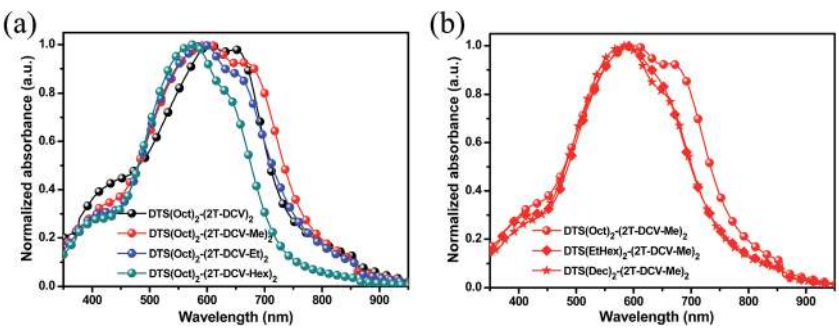

Fig. 2 UV-vis absorption spectra of the DTS-based oligomer pristine film spin-coated from chloroform (a) with different alkyl terminal chains and (b) with different alkyl chains on the DTS core.

Table 2 Optical and electrochemical properties of the DTS-based oligomers

	UV-vis absorption spectra				Cyclic voltammetry		
	Solution[a]	Film[b]			Oxidation	Reduction	
Compounds	λ_{max} (nm)	λ_{max} (nm)	λ_{onset} (nm)	E_g^{optc} (eV)	φ_{ox}[d]/HOMO (V)/(eV)	φ_{red}[d]/LUMO (V)/(eV)	E_g^{ec} (eV)
DTS(Oct)$_2$-(2T-DCV)$_2$	560	606	753	1.65	0.92/−5.32	−0.95/−3.45	1.87
DTS(Oct)$_2$-(2T-DCV-Me)$_2$	542	604	777	1.60	0.86/−5.26	−1.06/−3.34	1.92
DTS(Oct)$_2$-(2T-DCV-Et)$_2$	542	594	766	1.62	0.92/−5.32	−1.01/−3.39	1.93
DTS(Oct)$_2$-(2T-DCV-Hex)$_2$	542	575	726	1.71	0.90/−5.30	−1,05/−3.35	1.95
DTS(EtHex)$_2$-(2T-DCV-Me)$_2$	542	588	758	1.64	0.92/−5.32	−1.01/−3.39	1.93
DTS(Dec)$_2$-(2T-DCV-Me)$_2$	542	585	758	1.64	0.92/−5.32	−1.03/−3.37	1.95

[a] Measured in chloroform solution. [b] Cast from chloroform solution. [c] Bandgap estimated from the onset wavelength (λ_{edge}) of the optical absorption: $E_g^{opt} = 1240/\lambda_{edge}$. [d] Standard formal reduction (φ_{red}) and oxidation (φ_{ox}) potentials *vs.* SCE obtained for films of the oligomers.

The electrochemical properties of the oligomers were investigated using cyclic voltammetry (CV) (see Table 2 and Fig. S23–S25†). The results obtained demonstrate that all oligomers with alkyl-DCV groups possess similar electrochemical behavior. Their oxidation in a 1,2-dichlorobenzene–acetonitrile mixture occurs in two consecutive and fully reversible steps (Fig. S23†). Reduction proceeds also in two consecutive steps, where the first one is reversible while the second one is irreversible. However, in films the oxidation and reduction of these oligomers (see Fig. S24†) become quasi-reversible as compared to their solutions. This phenomenon can be attributed to the stacking of D–A oligothiophenes in the solid state.[29,34] The highest occupied molecular orbital (HOMO) and lowest unoccupied molecular orbital (LUMO) energy levels of the molecules with alkyl-DCV groups estimated from these data were very close, and were almost around −5.32 eV and −3.40 eV, respectively. This suggests that the variation of alkyl chains in donor and acceptor moieties has almost no influence on the energy levels of these molecules.

Interestingly we note that the absence of alkyl groups at the DCV unit does not influence the oxidation process and HOMO level, respectively (Table 2 and Fig. S25†). However, reduction of DTS(Oct)$_2$-(2T-DCV)$_2$ occurs at lower φ_{red} and was found to be irreversible both in solution and the film (Fig. S25†). This observation indicates that an alkyl chain on the DCV unit slightly hinders reduction of the DTS-based oligomer, but further stabilizes the anion radicals as compared to the common DCV groups having an active proton. DTS(Oct)$_2$-(2T-DCV)$_2$ has a reduced electrochemical bandgap (E_g^{ec}) value of 1.87 eV with a low-lying LUMO of −3.45 eV. Overall, high open circuit voltage (V_{oc}) values are expected for all of the DTS-based oligomer systems.[30]

2.4 Solar cell fabrication and performance

The device architectures and the schematic representation of the band energy diagrams for the conventional configuration of SMOCSs are shown in Fig. S26.† The detailed procedures for device fabrication can be found in the ESI.† The BHJ solar cells were first fabricated with a standard ITO/PEDOT:PSS/oligomer:PC$_{70}$BM/Ca/Al architecture. A range of active layer compositions (oligomer : PC$_{70}$BM ratios) was investigated systematically (see Fig. S27†). The relevant *J*–*V* characteristics of optimized devices and their PCEs as a function of molecular solubility are shown in Fig. S28.† On the one hand, similar oligomers show considerably different optimized D : A ratios and photovoltaic performances, as can be concluded from the data shown in Fig. S28† and Table 3. On the other hand, the relative device performance as a function of molecular solubility (see Fig. S28b†) is complex and not fully understood, although multiple studies reported that the solution evaporation rate does impact the crystallization kinetics of dominantly the donor phase.[18,35] It illustrates that a reasonable explanation of the device characteristics should consider simultaneously both the molecular solubility and morphology. Since these DTS-based oligomers show a similar HOMO energy level (see Table 2), the V_{oc} values for all of the devices are closely distributed around 0.90 V, with DTS(Oct)$_2$-(2T-DCV)$_2$ being the only exception. The lower V_{oc} of 0.78 V in DTS(Oct)$_2$-(2T-DCV)$_2$ device is in concordance with an overall low performance and is attributed to a poor blend morphology caused by the rather low solubility. Note that DTS(Oct)$_2$-(2T-DCV-Hex)$_2$ shows a slightly higher V_{oc} of up to 0.95 V, which suggests more isolated donor units and less donor–acceptor interactions originating from the longer alkyl chains.[4] Due to the various physical properties and morphological characteristics, these six DTS-based oligomers exhibited significantly different photovoltaic performances (see Table 3). DTS(Oct)$_2$-(2T-DCV-Me)$_2$ with methyl terminal groups shows the best device performance with a V_{oc} of 0.85 V, a short circuit current density (J_{sc}) of 8.7 mA cm^{-2}, a fill factor (FF) of 60.8%, and thus a PCE of 4.5%. We would like to stress that all solar cells were processed under environmental conditions. Processing under nitrogen may result in higher performance numbers of over 5%,[18,30] since the residual solvents in a glovebox may induce unexpected SVA.

Table 3 The photovoltaic parameters from *J*–*V* characteristics of optimized solar cells based on DTS-based oligomers as donors without or with SVA treatments

Blend films (D : A, wt%)	SVA (60 s)	V_{oc} [V]	J_{sc} [mA cm^{-2}]	J_{sc}[a] [mA cm^{-2}]	FF [%]	PCE[d] [%]
DTS(Oct)$_2$-(2T-DCV)$_2$: PC$_{70}$BM (1 : 2.5)	WO	0.78	3.5	2.6	40.4	1.1 (1.0)
	W	0.84	4.0	2.8	43.1	1.5 (1.2)
DTS(Oct)$_2$-(2T-DCV-Me)$_2$: PC$_{70}$BM (1 : 0.8)	WO	0.85	8.7	7.7	60.8	4.5 (4.4)
	W	0.90	10.0	9.0	68.8	6.2 (6.0)
DTS(Oct)$_2$-(2T-DCV-Et)$_2$: PC$_{70}$BM (1 : 2)	WO	0.90	8.6	8.2	43.5	3.4 (3.0)
	W	0.90	8.8	8.6	52.9	4.2 (3.9)
DTS(Oct)$_2$-(2T-DCV-Hex)$_2$: PC$_{70}$BM (1 : 3)	WO	0.95	5.8	5.7	35.0	1.9 (1.7)
	W	0.15	3.6	3.5	32.4	0.18 (0.12)
DTS(EtHex)$_2$-(2T-DCV-Me)$_2$: PC$_{70}$BM (1 : 2.5)	WO	0.88	5.7	4.8	51.9	2.6 (2.4)
	W	0.90	7.2	5.8	62.8	4.1 (3.9)
DTS(Dec)$_2$-(2T-DCV-Me)$_2$: PC$_{70}$BM (1 : 0.5)	WO	0.84	8.0	7.0	53.7	3.6 (3.4)
	W	0.90	8.3	7.8	62.1	4.6 (4.4)
DTS(Oct)$_2$-(2T-DCV-Me)$_2$[b]	W	0.90	10.4	9.7	67.0	6.3 (6.1)
DTS(Oct)$_2$-(2T-DCV-Me)$_2$[c]	W	0.88	10.9	10.1	66.3	6.4 (6.2)

[a] Calculated J_{sc} from EQE measurements. [b] ZnO/Al as the cathode. [c] PDINO/Ag as the cathode. [d] The average values of PCEs calculated from over twelve devices.

Various processing techniques such as thermal annealing, solvent additives and SVA treatment were used in order to modify the BHJ morphologies in these systems and thus to optimize further their photovoltaic performance. However, only SVA treatment was found to be useful for improving the device performance of these oligomers with the exception of the DTS(Oct)$_2$-(2T-DCV-Hex)$_2$ system. Different duration times of SVA treatment allowed the control and optimization of the microstructure very effectively. As shown in Fig. 3a and Table 3, the photovoltaic properties of all systems except DTS(Oct)$_2$-(2T-DCV-Hex)$_2$ were improved by SVA treatment. The optimized device performance of DTS(Oct)$_2$-(2T-DCV-Me)$_2$: PC$_{70}$BM (1 : 0.8, wt%) was found after a 60 s SVA treatment in chloroform. A V_{oc} of 0.90 V, a J_{sc} of 10.0 mA cm^{-2}, and a FF of 68.8% resulted in a PCE of 6.20% and thus an almost 40% performance increase. Depending on the alkyl chain length and the corresponding solubility, we found different trends. As exhibited in Fig. S29,† DTS(Oct)$_2$-(2T-DCV)$_2$ shows more or less the same performance independent of the SVA duration. Differently, for the DTS(Oct)$_2$-(2T-DCV-Hex)$_2$ system with hexyl terminal chains, we found that even the shortest SVA periods significantly dilapidate the BHJ morphology and result in reduced photovoltaic performance. The high molecular solubility of DTS(Oct)$_2$-(2T-DCV-Hex)$_2$ (24 mg mL^{-1}), which is very close to that of PC$_{70}$BM (30 mg mL^{-1}), is suggested as a limiting factor for SVA. As a result, DTS(Oct)$_2$-(2T-DCV-Hex)$_2$-based solar cells treated for 60 s with a SVA process demonstrate a dramatically low V_{oc} of 0.15 V, a J_{sc} of 3.6 mA cm^{-2}, and thus an overall PCE of only 0.18%. These three case studies strongly suggest that the relative molecular solubility of the donor and acceptor components play a crucial role in the functionality and methodology of the SVA treatment.

Next, we investigated the n-type interface to accomplish highly efficient and stable small molecule device architectures (see Fig. S26†). The DTS(Oct)$_2$-(2T-DCV-Me)$_2$ device based on a ZnO/Al cathode shows a slightly higher PCE of 6.3% as compared to that of the Ca/Al device (see Fig. 3c and Table 3). In comparison with Ca, the ZnO layer as the ETL exhibits better air stability. Nevertheless, the stability of the ZnO/Al based device is still quite poor owing to the instable Al cathode.[23] In the previous studies we have already demonstrated DMAPA-C$_{60}$ as a promising interlayer being compatible to a Ag cathode.[23] Here we introduced a new interfacial layer (PDINO) to modify the stable Ag cathode for expanding the currently rather limited choice of available electron transporting layers (ETLs) for small molecule OSCs (see Fig. S26†). As shown in Table 3, the DTS(Oct)$_2$-(2T-DCV-Me)$_2$ based device with a PDINO/Ag cathode shows the same if not even slightly higher PCE of 6.4% as compared to those devices based on air instable Ca/Ag and ZnO/Al cathodes. The tentatively slight improvement in performance is mainly attributed to the higher J_{sc} value (10.9 mA cm^{-2}) and underlines that the PC$_{70}$BM–PDINO–Ag interfaces do not suffer from energetic barriers.[20,36,37] EQE measurements confirm the small but distinct J_{sc} increase for DTS(Oct)$_2$-(2T-DCV-Me)$_2$ based devices in comparison to the various other cathodes mentioned above. Besides the efficiency improvement, the increased device stability was also observed, as expected, for the PDINO/Ag based conventional device (see Fig. S30†). Due to the high reactivity of the low work function Ca and Al with oxygen and moisture in the atmosphere, the PCE decreased dramatically for the device fabricated with Ca/Al and ZnO/Al as cathodes. In comparison, the PDINO/Ag based devices exhibited higher stability, illustrating that the PDINO layer can significantly improve the stability of the device with high work function Ag cathode.

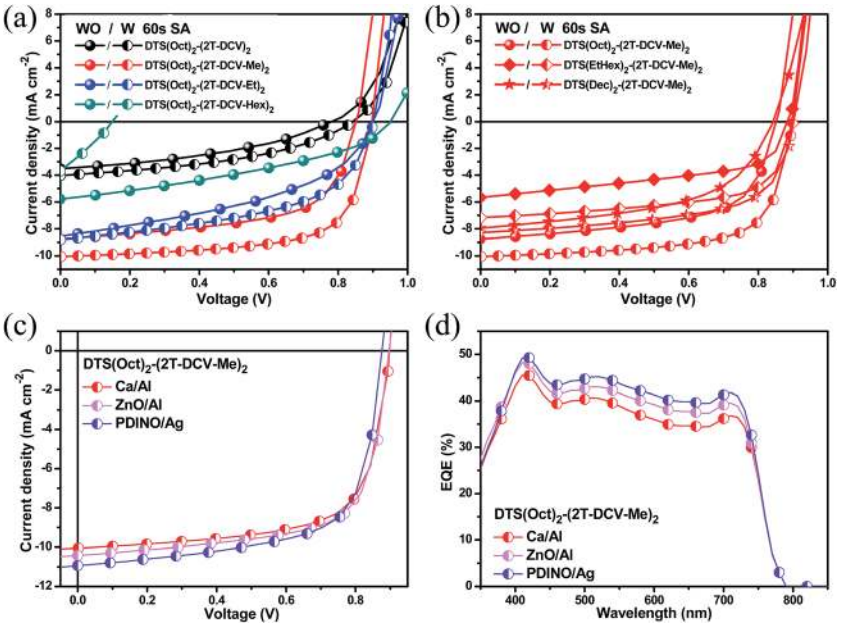

Fig. 3 J–V characteristics of optimized solar cells based on the oligomers with (a) different alkyl terminal chains and (b) different alkyl chains in donor units, measured under 100 mW cm^{-2} AM 1.5 G illumination; (c) J–V characteristics and (d) EQE spectra of DTS(Oct)$_2$-(2T-DCV-Me)$_2$-: PC$_{70}$BM (1 : 0.8, wt%) BHJ solar cells with SVA processes fabricated using Ca/Al, ZnO/Al, and PDINO/Ag as cathodes, respectively.

2.5 Film microstructure, morphology and phase separation

Before discussing the morphology, we first present the optical absorption spectra of the DTS-based oligomer blend films prepared on glass substrates as well as the EQE spectra of the various DTS-based oligomer based devices with and without SVA treatments (see Fig. S31†). The absorption spectra of the BHJ blends show a significant blue shift as compared to the spectra from the pristine DTS-based oligomer films. Obviously, $PC_{70}BM$ is disturbing the molecular ordering of the oligomers. However, a proper SVA treatment (Fig. S31†) is able to gain back molecular ordering and results in a red shift of the absorption spectrum (with the exception of $DTS(Oct)_2$-$(2T\text{-}DCV)_2$ and $DTS(Oct)_2$-$(2T\text{-}DCV\text{-}Hex)_2$). The same trend holds for the EQE data (see Fig. S31† and the detailed discussions therein) and confirms that SVA indeed facilitates reordering if not even recrystallization of the donor phases.

The blend surface morphology images of the six DTS-based oligomers were first investigated by atomic force microscopy (AFM) (see Fig. 4). Similar DTS-based oligomers exhibited huge differences for their surface morphologies, which can be attributed to the difference in the intermolecular interactions in these oligomers, which was indirectly revealed by their different molecular solubility values, phase behavior and solid-state absorption of pristine oligomers, as well as poor film-forming characteristics as discussed in our previous results.[4,5,18] The root-mean-square (RMS) roughness for these films is typically in the range of 0.5–1.5 nm, with the exception of the $DTS(Oct)_2$-$(2T\text{-}DCV)_2$ blend film with a RMS of 11.5 nm. The low molecular solubility of $DTS(Oct)_2$-$(2T\text{-}DCV)_2$ obviously worsen the film forming properties for the doctor-blading process. Consistent with the other findings further SVA treatment does not influence the film quality (see Fig. 4g). $DTS(Oct)_2$-$(2T\text{-}DCV\text{-}Hex)_2$, which suffered from too high solubility, forms noticeably large domain features with a RMS of 49.7 nm upon SVA (Fig. 4j). For the other four oligomers, we found that $PC_{70}BM$ causes a slightly higher roughness after the SVA treatment, with RMS values of 1.1–5.3 nm. Due to the suitable molecular solubility (5–14 mg mL^{-1}), AFM images of these four blended films reveal similar trends, with nanoscale phase separation and bicontinuous network formation upon SVA treatment. While we do not want to overstress the relevance of AFM studies to analyze the microstructure, we nevertheless state that the observed surface property trends fit well to the other data acquired so far. SVA plays a decisive role in the morphological revolution and device performance. To finalize these discussions we note that a 5 min SVA treatment of the $DTS(Oct)_2$-$(2T\text{-}DCV\text{-}Me)_2$ blend exhibited a more rough surface (a RMS of 4.53 nm) with increased domains (see Fig. S32†) resulting in worse photovoltaic performance as expected (see Fig. S29b†).

Grazing-Incidence Wide-Angle X-ray Scattering (GIWAXS) was further used to examine the thin film microstructure of these DTS-based oligomers in optimized BHJ films with $PC_{70}BM$ (see Fig. 5 and S33†). The X-ray pattern of the as-prepared $DTS(Oct)_2$-$(2T\text{-}DCV)_2$:$PC_{70}BM$ film shows sharp reflections located along the meridional direction (Fig. S33a†). These peaks are attributed to the crystal structure of the donor molecules. In addition, two broad reflections at approximately 10.5 and 5.0 Å are identified. The latter corresponds to the most intense peak of the monoclinic $PC_{70}BM$ phase.[4,18] We suggest that $PC_{70}BM$ forms small irregular aggregates of poor crystallinity in the bulk heterojunction composites. After SVA, only the first order of the layered structure of the $DTS(Oct)_2$-$(2T\text{-}DCV)_2$ structure at 12.4 Å remains (*cf.* Fig. S33b†). The peak of $PC_{70}BM$ remains always unchanged.

SVA clearly increases the crystallinity of $DTS(Oct)_2$-$(2T\text{-}DCV\text{-}Me)_2$:$PC_{70}BM$ thin films (Fig. 5). Apart from the crystalline phase of the electron donor, the broad peaks of $PC_{70}BM$ are also visible. The parameters of the crystal phase are presented in our previous publication.[18] However, the diffractogram of a non-annealed sample with longer ethyl terminal groups, $DTS(Oct)_2$-$(2T\text{-}DCV\text{-}Et)_2$:$PC_{70}BM$, shows only the $PC_{70}BM$ reflections at approximately 10 and 4.9 Å (Fig. S33c†). This means that the crystalline structure of $DTS(Oct)_2$-$(2T\text{-}DCV\text{-}Et)_2$ was not formed. After annealing, weak peaks at 15 and 7.9 Å appear and indicate the formation of the $DTS(Oct)_2$-$(2T\text{-}DCV\text{-}Et)_2$ crystalline phase (Fig. S33d†). Further elongation of the terminal alkyl groups from ethyl to hexyl results in a failure of the SVA process to form ordered phases of the oligomer, and only reflections of $PC_{70}BM$ are observed (Fig. S33e and S33f†).

The behavior of $PC_{70}BM$ blends either with $DTS(EtHex)_2$-$(2T\text{-}DCV\text{-}Me)_2$ (Fig. S33g and S33h†) or $DTS(Dec)_2$-$(2T\text{-}DCV\text{-}Me)_2$ (Fig. S33i and S33j†) is similar to that found for the film of their homologue with central octyl groups ($DTS(Oct)_2$-$(2T\text{-}DCV\text{-}Me)_2$:$PC_{70}BM$). The SVA stimulates an enhancement of both crystalline phases, which were presented already in the non-annealed samples. Importantly, for these three samples with methyl terminal groups, the films after SVA display a reflection at 3.8 Å located near the equator of the pattern. This peak can be attributed to π–π stacking of the conjugated cores. Based on the X-ray patterns, one can conclude that the $DTS(Dec)_2$-$(2T\text{-}DCV\text{-}Me)_2$:$PC_{70}BM$ film forms the most ordered structure. The films before and after SVA exhibit a well-organized and crystalline structure (Fig. S33i and S33j†). Using the experimental *d*-spacings and azimuthal peak positions, the reflections were indexed to a monoclinic unit cell (Table S1†): the symmetry is $P21/n$, and the unit cell parameters are $a = 21.63$ Å; $b = 9.01$ Å; $c = 30.75$ Å; $\beta = 109.4°$. We suppose that the structure is similar to that discussed in the literature for 5,5-bis{7-(4-(thiophen-2-yl))-[1,2,5]thiadiazolo[3,4-*c*]pyridine}-3,3′-di-2-ethylhexylsilylene-2,2′-bithiophene with a close molecular architecture.[38] We summarize the microstructure investigations with concluding that the SVA process plays an important role in enhancing the formation of crystalline structures within the blend composite films (Table S2†). It is further important to note that the two broad peaks at *ca.* 10 and 5 Å, representing $PC_{70}BM$, are only minorly influenced by the SVA process. Moreover, the nature of the substrate does not influence significantly the blend morphology (see Fig. S34 and Table S3†).

In recent studies, the SVA approach was shown to successfully improve the morphologies of selected BHJ films by increasing the aggregation of the donors and acceptors and/or forming nanodomains of the pure phase as well as improving vertical concentration profiles within the active layer.[12,17,39,40] A

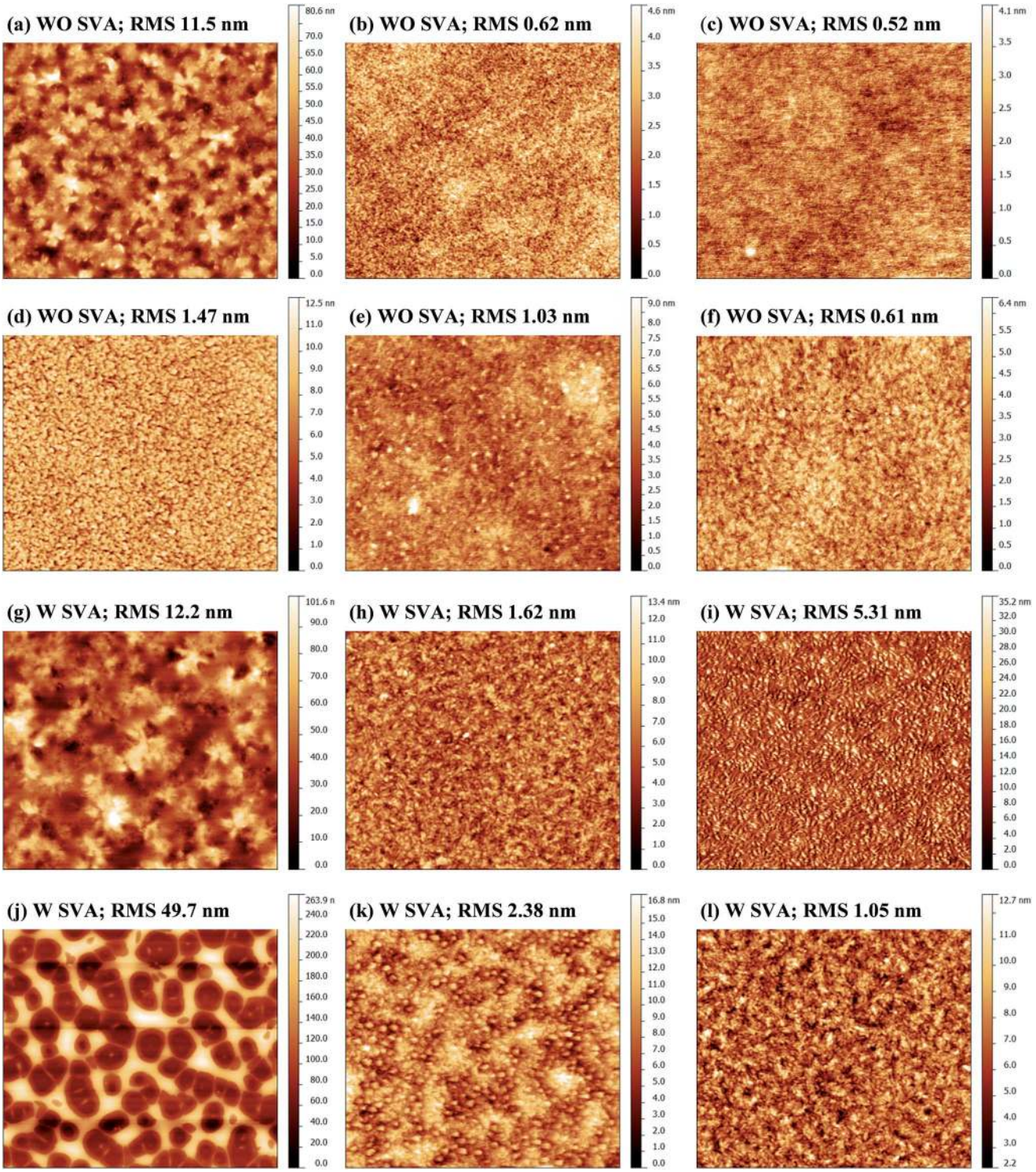

Fig. 4 AFM topography images of DTS-based oligomer blend films without and with the 60 s SVA process of (a and g) DTS(Oct)$_2$-(2T-DCV)$_2$, (b and h) DTS(Oct)$_2$-(2T-DCV-Me)$_2$, (c and i) DTS(Oct)$_2$-(2T-DCV-Et)$_2$, (d and j) DTS(Oct)$_2$-(2T-DCV-Hex)$_2$, (e and k) DTS(EtHex)$_2$-(2T-DCV-Me)$_2$, (f and l) DTS(Dec)$_2$-(2T-DCV-Me)$_2$. (a–f) show blend films without the 60 SVA process while (g–l) show the related films with the 60 s SVA process. The scanning area is 5 × 5 μm^2 for all images.

simple approach to predict the blend morphology as a linear function of the material solubility in blends is typically not sufficient to explain the impact of the SVA method on SMOSCs. Our results for the DTS series give a more mixed picture. DTS(Oct)$_2$-(2T-DCV-Hex)$_2$ with the highest solubility (*i.e.* 24 mg mL^{-1} which is close to that of PC$_{70}$BM with 30 mg mL^{-1}) is negatively impacted by the SVA treatment leading to a rough blend morphology with a wide distribution of domain sizes (see

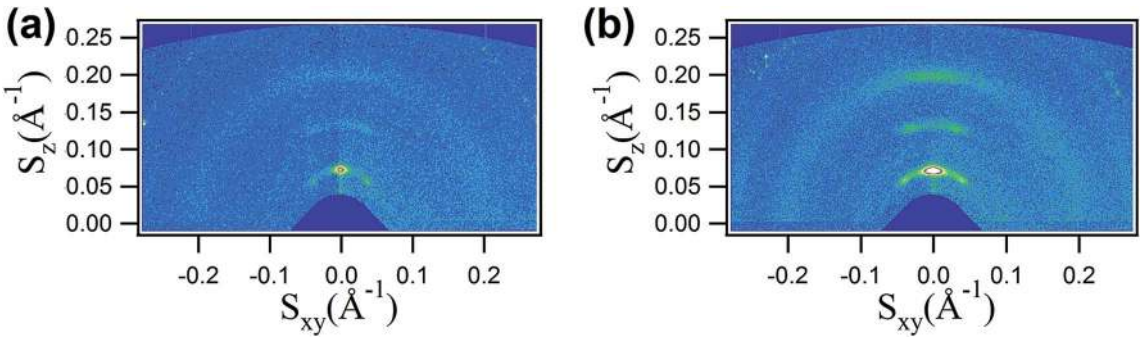

Fig. 5 2D GIWAXS patterns of the DTS(Oct)$_2$-(2T-DCV-Me)$_2$:PC$_{70}$BM blended film: before (a) and (b) after SVA.

Fig. 4d and j). In contrast, SVA treatments work properly for the other DTS-based oligomers with lower solubilities (5–14 mg mL^{-1}) and result in enhanced crystallinity of donor phases (Fig. 4). Bäuerle *et al.* demonstrated that oligomers with significantly higher molecular solubility (>66 mg mL^{-1}) than PCBM again benefit from a SVA treatment.[12] Therefore, our initial conclusion is that a distinct solubility difference between the donor and acceptor plays a vital role for a successful SVA treatment.

2.6 Charge carrier mobility

In order to further understand the relationship between the charge carrier transport properties and the blend morphologies we determined the charge carrier mobilities from space charge limited current (SCLC) measurements on representative thin film devices, as shown in Fig. 6 and Table S4† (the fitting curves are exhibited in Fig. S35†). For DTS-based oligomers with various alkyl terminal lengths, the hole mobility in blends gradually decreases with the increase of the alkyl chain length. This fact can be explained by weaker intermolecular interactions in films for molecules having longer alkyl chains, which is also in agreement with the phase behavior (see Table 1), absorption spectra (see Fig. 2), AFM and GIWAXS, as well as our previous results.[4,18] After SVA treatments, all blends of the oligomers with PC$_{70}$BM show higher hole mobilities, with the exception of the DTS(Oct)$_2$-(2T-DCV-Hex)$_2$ system (see Fig. 6). In direct contrast to that, the mobility of DTS(Oct)$_2$-(2T-DCV-Hex)$_2$ blends deteriorate by approximately one order in magnitude after the SVA treatment. The charge transport properties in blends with and without SVA treatments were next examined in electron only devices. The electron mobility (μ_e) in blends after SVA treatments is more or less higher than those of blends without SVA treatment (see Fig. 6 and Table S4†). Apart from the enhanced charge transport properties after SVA treatment, we next investigate the impact on the recombination losses.

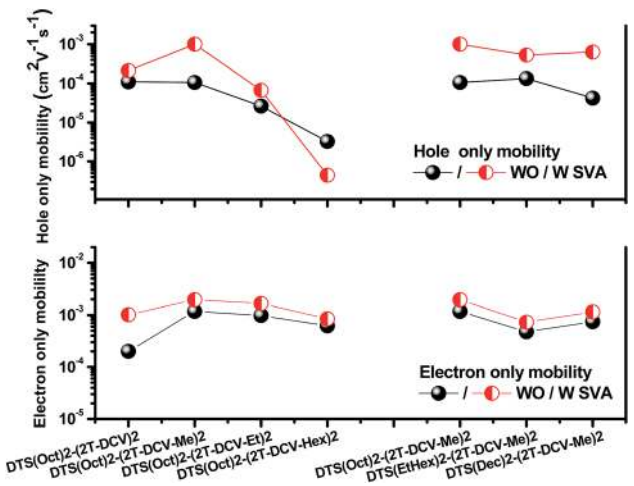

Fig. 6 Hole-only mobility and electron-only mobility of the DTS-based oligomer based blends without and with 60 s SVA treatments.

2.7 Non-geminate recombination dynamics

To further gain insight into the influence of the blend morphology and charge transport caused by the various alkyl chains and SVA treatments on the device performance, here we studied the light intensity dependence of *J–V* characteristics.[41,42] The *J–V* characteristics of the DTS(Oct)$_2$-(2T-DCV-Me)$_2$:PC$_{70}$BM and DTS(Oct)$_2$-(2T-DCV-Hex)$_2$:PC$_{70}$BM devices with and without SVA treatments under illumination intensities ranging from 100 to 1 mW cm^{-2} are shown in Fig. S36.† The light intensity dependence of J_{sc} and V_{oc} is presented and plotted in Fig. 7a and b, respectively. Note that the relative light intensity dependent data of the DTS(Oct)$_2$-(2T-DCV-Hex)$_2$:PC$_{70}$BM device after SVA treatment were strongly affected by the deteriorated worse device performance with a V_{oc} of *ca.* 0.15 V (see Table 3). As shown in Fig. 7a, the slope (α) of the DTS(Oct)$_2$-(2T-DCV-Me)$_2$:PC$_{70}$BM device without SVA treatment is 1.02, whereas that of the DTS(Oct)$_2$-(2T-DCV-Hex)$_2$:PC$_{70}$BM device is only 0.92 (ref. 18). After SVA treatment, the DTS(Oct)$_2$-(2T-DCV-Me)$_2$:PC$_{70}$BM device exhibits the same slope (α) values. It indicates that the carrier sweep-out is most efficient and 2nd order recombination effects are suppressed in the presence of a built in field.[18,41] SVA treatment only slightly influences the charge extraction in DTS(Oct)$_2$-(2T-DCV-Me)$_2$:PC$_{70}$BM blends. In contrast, the slopes of V_{oc} *versus* ln(I) for the DTS(Oct)$_2$-(2T-DCV-Me)$_2$ system change from 1.21 kT/q to 1.03 kT/q upon SVA treatment, respectively. It implies that the SVA treatment effectively does reduce the number of microstructure induced recombination centers in the DTS(Oct)$_2$-(2T-DCV-Me)$_2$ device.

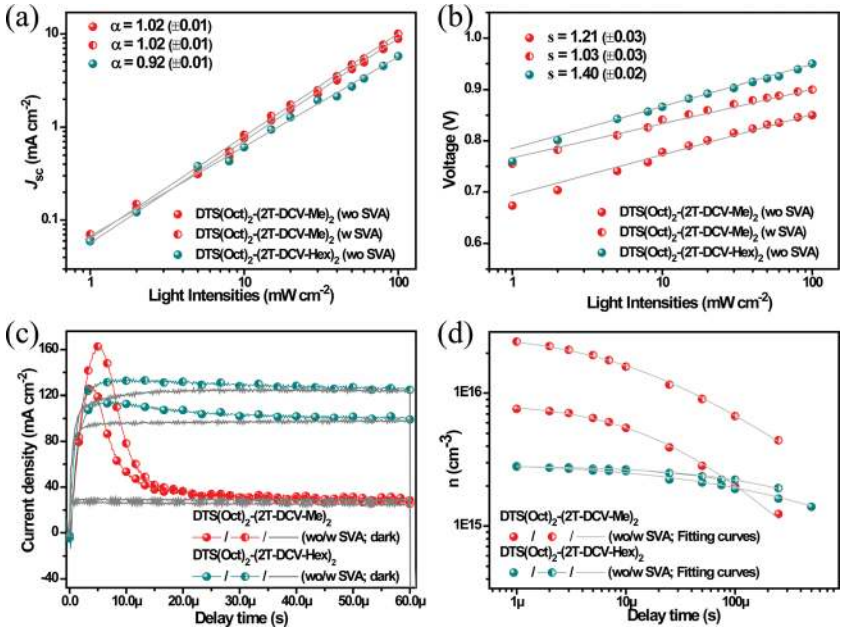

Fig. 7 The measured (a) J_{sc} and (b) V_{oc} of DTS(Oct)$_2$-(2T-DCV-Me)$_2$:PC$_{70}$BM and DTS(Oct)$_2$-(2T-DCV-Hex)$_2$:PC$_{70}$BM solar cells with and without SVA treatments as a function of illumination intensity, together with linear fits to the relative data (solid lines). (c) The Photo-CELIV traces for the DTS(Oct)$_2$-(2T-DCV-Me)$_2$:PC$_{70}$BM and DTS(Oct)$_2$-(2T-DCV-Hex)$_2$:PC$_{70}$BM solar cells with and without SVA treatments after a delay time of 1 μs. The dark CELIV traces are also shown; (d) numbers of extracted carriers as a function of delay time and the fit.

Besides that, we also fitted the J_{sc} and V_{oc} *versus* light intensity relationship for other systems under various light intensities, as shown in Fig. S37† (DTS(Oct)$_2$-(2T-DCV-Et)$_2$ system), Fig. S38† (DTS(EtHex)$_2$-(2T-DCV-Me)$_2$ system), and Fig. S39† (DTS(Dec)$_2$-(2T-DCV-Me)$_2$ system), respectively. All of these data illustrate that the slopes (α) of J_{sc} *versus* ln(I) are more close to unity after SVA treatment, underlining reduced bimolecular recombination during the sweep-out.[18] More general, the relative slopes (kT/q) of V_{oc} *versus* ln(I) quite significantly decrease upon SVA due to the better BHJ microstructure after annealing.[43]

Finally, photo-CELIV was applied to analyze the charge carrier transport and relative recombination mechanisms in these systems (see Fig. S40–S43†). Over ten photo-CELIV curves have been recorded using different experimental conditions for each sample, differing in delay time and applied voltage. Fig. 7c and d show the photocurrent transients recorded by applying a 2 V/60 μs linearly increasing reverse bias pulse to the devices based on DTS(Oct)$_2$-(2T-DCV-Me)$_2$:PC$_{70}$BM and DTS(Oct)$_2$-(2T-DCV-Hex)$_2$:PC$_{70}$BM without and with SVA treatments after a 1 μs delay time. The average mobility of the DTS(Oct)$_2$-(2T-DCV-Me)$_2$:PC$_{70}$BM device with SVA treatment (1.06×10^{-4} cm^2 V^{-1} s^{-1}) is higher than that of the device without SVA treatment (6.35×10^{-5} cm^2 V^{-1} s^{-1}) (see Table S5†). In contrast, the DTS(Oct)$_2$-(2T-DCV-Hex)$_2$:PC$_{70}$BM device with SVA treatment exhibits a lower mobility of 9.28×10^{-6} cm^2 V^{-1} s^{-1} as compared to the untreated device (1.67×10^{-5} cm^2 V^{-1} s^{-1}). In addition, the other systems including DTS(Oct)$_2$-(2T-DCV-Et)$_2$, DTS(EtHex)$_2$-(2T-DCV-Me)$_2$, and DTS(Dec)$_2$-(2T-DCV-Me)$_2$ also show the higher charge carrier mobility in devices with SVA treatments (see Table S5†).

The time-dependence of the charge carrier density was further studied in order to investigate the recombination mechanisms in these systems. From the fit to relative eqn (1),[18]

$$n(t) = \frac{n(0)}{1 + \left(\frac{t}{\tau_B}\right)^{\gamma}} \quad (1)$$

the effective 2nd order recombination coefficient (τ_B), the initial density of photogenerated carriers ($n(0)$) and the time independent parameter (γ) values of these systems are summarized in Table S5.† The carrier densities of the DTS-based oligomer based devices, with the exception of the DTS(Oct)$_2$-(2T-DCV-Hex)$_2$ system, were more or less improved by SVA treatments. Furthermore, the reduced τ_B and shorter transient time (t_{tr}) values[18] indicate that a lower density of trapping states exists in SVA treated systems, again with the exception of the DTS(Oct)$_2$-(2T-DCV-Hex)$_2$. Besides, using these photo-CELIV mobility values,[18] we further calculated the Langevin recombination coefficients (β_L) in these systems. The related results finally underline the trends reported for the morphological characteristics, charge transport properties, recombination loss mechanisms as well as the photovoltaic performance as we discussed earlier.

3. Conclusion

A series of novel linear A–π–D–π–A oligomers, having a central electron-donating DTS unit linked through a bithiophene π-bridge with terminal electron-withdrawing either alkyl-DCV or DCV groups, were designed and synthesized to systematically study the structure–property relationships depending on the

type of acceptor and alkyl group. The investigations demonstrated a number of benefits to use alkyl-DCV groups instead of common DCV ones for the design of D–A oligomers, such as higher solubility, electrochemical stability and photovoltaic performance. The physical properties of the oligomers revealed that the alkyl chains have also a significant impact on intramolecular and intermolecular interactions affecting various solid-state properties of pristine oligomers and their blends with $PC_{70}BM$. Elongation and branching of alkyl groups at the central DTS or terminal DCV unit reduces intermolecular interactions, which in turn increases molecular solubility of the oligomers, but decreases their crystallinity, absorption in the long-wave region, and charge carrier mobility in blends. Furthermore, the photovoltaic properties of these devices, with the exception of the $DTS(Oct)_2$-$(2T\text{-}DCV\text{-}Hex)_2$ system, were improved by SVA treatments. After applying morphological and interfacial engineering $DTS(Oct)_2$-$(2T\text{-}DCV\text{-}Me)_2/PC_{70}BM$ composites give PCEs of over 6% for Ca/Al, ZnO/Al or PDINO/Ag cathodes. Finally, a more detailed study of the morphology–property relationships for these DTS-based oligomers was discussed to elucidate the correlation between the morphological modifications, charge transport properties and recombination loss mechanisms. All these data consistently underline that SVA treatment is suitable to optimize the film microstructure of OSCs based on small molecules as long as the molecular solubility of the donor is sufficiently different from that of the acceptor. We envisage that these concepts and this insight into the structure–morphology–property relationship will guide the development of novel molecules reaching a record-breaking efficiency under practical conditions.

Acknowledgements

The authors would like to thank Xuechen Jiao and Prof. Harald Ade (Department of Physics North Carolina State University, North Carolina, USA) for the preliminary study of the SVA effect by soft X-ray scattering (RSoXS) measurements. The authors also gratefully acknowledge the support of the Cluster of Excellence "Engineering of Advanced Materials" at the University of Erlangen-Nuremberg, which is funded by the German Research Foundation (DFG) within the framework of its "Excellence Initiative". The part of this work including the design, synthesis and characterization of the DTS-based oligomers with alkyl-DCV groups was carried out under financial support from the Russian Foundation for Basic Research (grant No.15-33-20957), whereas synthesis and characterization of $DTS(Oct)_2$-$(2T\text{-}DCV)_2$ has been funded by the Program of President of Russian Federation for Support of Young Scientists (grant MK-5061.2015.3). The work has been also partially funded by the Sonderforschungsbereich 953 "Synthetic Carbon Allotropes", the China Scholarship Council (CSC). We also thank the support of Solar Technologies go Hybrid (SolTech) project. D. V. Anokhin and D. A. Ivanov acknowledge the Russian Ministry of Science and Education (project for financial support of leading scientists No.11.G34.31.0055 from 19.10.2011).

References

1 Y. S. Chen, X. J. Wan and G. K. Long, *Acc. Chem. Res.*, 2013, **46**, 2645–2655.
2 Q. Zhang, B. Kan, F. Liu, G. Long, X. Wan, X. Chen, Y. Zuo, W. Ni, H. Zhang, M. Li, Z. Hu, F. Huang, Y. Cao, Z. Liang, M. Zhang, T. P. Russell and Y. Chen, *Nat. Photonics*, 2015, **9**, 35–41.
3 K. Sun, Z. Xiao, S. Lu, W. Zajaczkowski, W. Pisula, E. Hanssen, J. M. White, R. M. Williamson, J. Subbiah, J. Ouyang, A. B. Holmes, W. W. H. Wong and D. J. Jones, *Nat. Commun.*, 2015, **6**, 6013.
4 J. Min, Y. N. Luponosov, A. Gerl, M. S. Polinskaya, S. M. Peregudova, P. V. Dmitryakov, A. V. Bakirov, M. A. Shcherbina, S. N. Chvalun, S. Grigorian, N. Kausch-Busies, S. A. Ponomarenko, T. Ameri and C. J. Brabec, *Adv. Energy Mater.*, 2014, **4**, 1301234.
5 J. Min, Y. N. Luponosov, D. Baran, S. N. Chvalun, M. A. Shcherbina, A. V. Bakirov, P. V. Dmitryakov, S. M. Peregudova, N. Kausch-Busies, S. A. Ponomarenko, T. Ameri and C. J. Brabec, *J. Mater. Chem. A*, 2014, **2**, 16135.
6 J. Roncali, P. Leriche and P. Blanchard, *Adv. Mater.*, 2014, **26**, 3821–3838.
7 W. Ni, X. J. Wan, M. M. Li, Y. C. Wang and Y. S. Chen, *Chem. Commun.*, 2015, **51**, 4936–4950.
8 Z. G. Zhang, J. Min, S. Y. Zhang, J. Zhang, M. J. Zhang and Y. F. Li, *Chem. Commun.*, 2011, **47**, 9474–9476.
9 D. Deng, Y. Zhang, L. Yuan, C. He, K. Lu and Z. Wei, *Adv. Energy Mater.*, 2014, **4**, 1400538.
10 S. L. Shen, P. Jiang, C. He, J. Zhang, P. Shen, Y. Zhang, Y. P. Yi, Z. J. Zhang, Z. B. Li and Y. F. Li, *Chem. Mater.*, 2013, **25**, 2274–2281.
11 Y. Zhang, C. K. Kim, J. Lin and T.-Q. Nguyen, *Adv. Funct. Mater.*, 2012, **22**, 97–105.
12 (*a*) C. D. Wessendorf, G. L. Schulz, A. Mishra, P. Kar, I. Ata, M. Weidelener, M. Urdanpilleta, J. Hanisch, E. Mena-Osteritz, M. Lindén, E. Ahlswede and P. Bäuerle, *Adv. Energy Mater.*, 2014, **4**, 1400266; (*b*) S. Roquet, A. Cravino, P. Leriche, O. Aleveque, P. Frere and J. Roncali, *J. Am. Chem. Soc.*, 2006, **128**, 3459–3466.
13 J. Min, Y. N. Luponosov, T. Ameri, A. Elschner, S. M. Peregudova, D. Baran, T. Heumüller, N. Li, F. Machui, S. Ponomarenko and C. J. Brabec, *Org. Electron.*, 2013, **14**, 219–229.
14 I. Burgués-Ceballos, F. Machui, J. Min, T. Ameri, M. M. Voigt, Y. N. Luponosov, S. A. Ponomarenko, P. D. Lacharmoise, M. Campoy-Quiles and C. J. Brabec, *Adv. Funct. Mater.*, 2014, **24**, 1449–1457.
15 J. Kong, I.-W. Hwang and K. Lee, *Adv. Mater.*, 2014, **26**, 6275–6283.
16 G. Lakhwani, A. Rao and R. H. Friend, *Annu. Rev. Phys. Chem.*, 2014, **65**, 557–581.
17 B. Kan, Q. Zhang, M. Li, X. Wan, W. Ni, G. Long, Y. Wang, X. Yang, H. Feng and Y. Chen, *J. Am. Chem. Soc.*, 2014, **136**, 15529–15532.

18 J. Min, Y. N. Luponosov, N. Gasparini, M. Richter, A. V. Bakirov, M. A. Shcherbina, S. N. Chvalun, L. Grodd, S. Grigorian, T. Ameri, S. A. Ponomarenko and C. J. Brabec, *Adv. Energy Mater.*, 2015, **5**, 1500386.
19 J. Reinhardt, M. Grein, C. Bühler, M. Schubert and U. Würfel, *Adv. Energy Mater.*, 2014, **4**, 1400081.
20 J. Min, Z.-G. Zhang, Y. Hou, C. O. Ramirez Quiroz, T. Przybilla, C. Bronnbauer, F. Guo, K. Forberich, H. Azimi, T. Ameri, E. Spiecker, Y. Li and C. J. Brabec, *Chem. Mater.*, 2015, **27**, 227–234.
21 C.-C. Chueh, C.-Z. Li and A. K.-Y. Jen, *Energy Environ. Sci.*, 2015, **8**, 1160–1189.
22 A. K. K. Kyaw, D. H. Wang, D. Wynands, J. Zhang, T.-Q. Nguyen, G. C. Bazan and A. J. Heeger, *Nano Lett.*, 2013, **13**, 3796–3801.
23 J. Min, Y. N. Luponosov, Z.-G. Zhang, S. A. Ponomarenko, T. Ameri, Y. F. Li and C. J. Brabec, *Adv. Energy Mater.*, 2014, **4**, 1400816.
24 H. Meier, *Angew. Chem., Int. Ed.*, 2005, **44**, 2482–2506.
25 L. J. Huo, H.-Y. Chen, J. H. Hou, T. L. Chen and Y. Yang, *Chem. Commun.*, 2009, 5570–5572.
26 S. Barlow, S. A. Odom, K. Lancaster, Y. A. Getmanenko, R. Mason, V. Coropceanu, J.-L. Brédas and S. R. Marder, *J. Phys. Chem. B*, 2010, **114**, 14397–14407.
27 S. A. Ponomarenko, Y. N. Luponosov, J. Min, A. N. Solodukhin, N. Surin, M. A. Shcherbina, S. N. Chvalun, T. Ameri and C. J. Brabec, *Faraday Discuss.*, 2014, **174**, 313–339.
28 J. Min, Y. N. Luponosov, D. Baran, S. N. Chvalun, M. A. Shcherbina, A. V. Bakirov, P. V. Dmitryakov, S. M. Peregudova, N. Kausch-Busies, S. A. Ponomarenko, T. Ameri and C. J. Brabec, *J. Mater. Chem. A*, 2014, **2**, 16135–16147.
29 Y. N. Luponosov, J. Min, A. V. Bakirov, P. V. Dmitryakov, S. N. Chvalun, S. M. Peregudova, T. Ameri, C. J. Brabec and S. A. Ponomarenko, *Dyes Pigm.*, 2015, **122**, 213–223.
30 Y. N. Luponosov, J. Min, T. Ameri, C. J. Brabec and S. A. Ponomarenko, *Org. Electron.*, 2014, **15**, 3800–3804.
31 Y. N. Luponosov, J. Min, D. A. Khanin, D. Baran, S. A. Pisarev, S. M. Peregudova, P. V. Dmitryakov, S. N. Chvalun, G. V. Cherkaev, E. A. Svidchenko, T. Ameri, C. J. Brabec and S. A. Ponomarenko, *J. Photonics Energy*, 2015, **5**, 057213.
32 D. V. Anokhin, M. Defaux, A. Mourran, M. Moeller, Y. N. Luponosov, O. V. Borshchev, A. V. Bakirov, M. A. Shcherbina, S. N. Chvalun, T. Meyer-Friedrichsen, A. Elschner, S. Kirchmeyer, S. A. Ponomarenko and D. A. Ivanov, *J. Phys. Chem. C*, 2012, **116**, 22727–22736.
33 J. Min, Z. G. Zhang, S. Y. Zhang, M. J. Zhang, J. Zhang and Y. F. Li, *Macromolecules*, 2011, **44**, 7632–7638.
34 Y. Liu, X. Wan, F. Wang, J. Zhou, G. Long, J. Tian, J. You, Y. Yang and Y. Chen, *Adv. Energy Mater.*, 2011, **1**, 771–775.
35 G. Li, Y. Yao, H. Yang, V. Shrotriya, G. Yang and Y. Yang, *Adv. Funct. Mater.*, 2007, **17**, 1636–1644.
36 Z. A. Page, Y. Liu, V. V. Duzhko, T. P. Russell and T. Emrick, *Science*, 2014, 1255826.
37 Z.-G. Zhang, B. Y. Qi, Z. W. Jin, D. Chi, Z. Qi, Y. F. Li and J. Z. Wang, *Energy Environ. Sci.*, 2014, **7**, 1966–1973.
38 G. C. Welch, L. A. Perez, C. V. Hoven, Y. Zhang, X.-D. Dang, A. Sharenko, M. F. Toney, E. J. Kramer, T.-Q. Nguyen and G. C. Bazan, *J. Mater. Chem.*, 2011, **21**, 12700–12709.
39 J. Liu, Q. Liang, H. Wang, M. Li, Y. Han, Z. Xie and L. Wang, *J. Phys. Chem. C*, 2014, **118**, 4585–4595.
40 B. Kan, M. Li, Q. Zhang, F. Liu, X. Wan, Y. Wang, W. Ni, G. Long, X. Yang, H. Feng, Y. Zuo, M. Zhang, F. Huang, Y. Cao, T. P. Russell and Y. Chen, *J. Am. Chem. Soc.*, 2015, **137**, 3886–3893.
41 V. D. Mihailetchi, L. J. A. Koster, J. C. Hummelen and P. W. M. Blom, *Phys. Rev. Lett.*, 2004, **93**, 216601.
42 S. M. Tuladhar, D. Poplavskyy, S. A. Choulis, J. R. Durrant, D. D. C. Bradley and J. Nelson, *Adv. Funct. Mater.*, 2005, **15**, 1171–1182.
43 L. J. A. Koster, V. D. Mihailetchi, R. Ramaker and P. W. M. Blom, *Appl. Phys. Lett.*, 2005, **86**, 123509.